
Generative Sliced MMD Flows with Riesz Kernels

Johannes Hertrich

TU Berlin

j.hertrich@math.tu-berlin.de

Christian Wald

TU Berlin

wald@math.tu-berlin.de

Fabian Altekrüger

Humboldt-Universität zu Berlin,

fabian.altekrueger@hu-berlin.de

Paul Hagemann

TU Berlin

hagemann@math.tu-berlin.de

Abstract

Maximum mean discrepancy (MMD) flows suffer from high computational costs in large scale computations. In this paper, we show that MMD flows with Riesz kernels $K(x, y) = -\|x - y\|^r$, $r \in (0, 2)$ have exceptional properties which allow their efficient computation. We prove that the MMD of Riesz kernels coincides with the MMD of their sliced version. As a consequence, the computation of gradients of MMDs can be performed in the one-dimensional setting. Here, for $r = 1$, a simple sorting algorithm can be applied to reduce the complexity from $O(MN + N^2)$ to $O((M + N) \log(M + N))$ for two measures with M and N support points. As another interesting follow-up result, the MMD of compactly supported measures can be estimated from above and below by the Wasserstein-1 distance. For the implementations we approximate the gradient of the sliced MMD by using only a finite number P of slices. We show that the resulting error has complexity $O(\sqrt{d/P})$, where d is the data dimension. These results enable us to train generative models by approximating MMD gradient flows by neural networks even for image applications. We demonstrate the efficiency of our model by image generation on MNIST, FashionMNIST and CIFAR10.

1 Introduction

With the rise of generative models, the field of gradient flows in measure spaces received increasing attention. Based on classical Markov chain Monte Carlo methods, Welling and Teh [75] proposed to apply the Langevin dynamics for inferring samples from a known probability density function. This corresponds to simulating a Wasserstein gradient flow with respect to the Kullback-Leibler divergence, see [36]. Closely related to this approach are current state-of-the-art image generation methods like score-based models [64, 65] or diffusion models [34, 66], which significantly outperform classical generative models like GANs [25] or VAEs [39]. A general aim of such algorithms [5, 34, 76] is to establish a path between input and target distribution, where "unseen" data points are established via the randomness of the input distribution.

For approximating gradient flows with respect to other functionals than the KL divergence, the authors of [1, 2, 21, 52] proposed the use of suitable forward and backward discretizations. To reduce the computational effort of evaluating distance measures on high-dimensional probability distributions, the sliced Wasserstein metric was introduced in [61]. The main idea of the sliced Wasserstein distance is to compare one-dimensional projections of the corresponding probability distributions instead of the distributions themselves. This approach can be generalized to more general probability metrics [42] and was applied in the context of Wasserstein gradient flows in [13, 50].

For many generative gradient-flow methods it is required that the considered functional can be evaluated based on samples. For divergence-based functionals like the Kullback-Leibler or the Jensen-Shannon divergence, a variational formulation leading to a GAN-like evaluation procedure is provided in [21]. In contrast, the authors of [1, 4, 24] use functionals based on the maximum mean discrepancy (MMD) which can be directly evaluated based on empirical measures. For positive definite kernels, it can be shown under some additional assumptions that MMD defines a metric on the space of probability distributions, see e.g., [28, 67, 68]. If the considered kernel is smooth, then Arbel et al. [4] proved that Wasserstein gradient flows can be fully described by particles. Even though this is no longer true for non-smooth kernels [32], Altekruiger et al. [1] pointed out that particle flows are Wasserstein gradient flows at least with respect to a restricted functional. In particular, we can expect that particle flows provide an accurate approximation of Wasserstein gradient flows as long as the number of particles is large enough.

Contributions. The computational complexity of MMD between two empirical measures with N and M support points depends quadratically on N and M , which makes large scale computations impossible. In this paper, we focus on the MMD with *Riesz kernels*

$$K(x, y) = -\|x - y\|^r, \quad r \in (0, 2), \quad (1)$$

also known as energy distance [63, 72]. We show that Riesz kernels have the outstanding property that their MMD coincides with the sliced MMD of univariate Riesz kernels. It is this property that enables us to reduce the computation of (gradients of) MMD to the one-dimensional setting. In the case of $r = 1$, we propose a simple and computationally very efficient sorting algorithm for computing the gradient of the one-dimensional MMD with complexity $O((M + N) \log(M + N))$. Our approach opens the door to applications in image processing, where we have usually to cope with high dimensional data.

In practice, sliced probability metrics are evaluated by replacing the expectation over all projections by the empirical expectation resulting in a finite sum. In the case of sliced MMD with Riesz kernels and $r = 1$, we prove that the error induced by this approximation behaves asymptotically as $O(\sqrt{d/P})$, where d is the data dimension and P the number of projections. The square root scaling of the error in the dimension d ensures that an accurate computation of the sliced MMD with Riesz kernels is possible even in very high dimensions. Taking into account the number of projections, the overall complexity of the computation of the derivatives of MMD is $O(dP(M + N) \log(M + N))$.

We apply the cheap evaluation of MMD gradients to compute MMD particle flows starting with samples from an initial probability measure μ_0 to samples from a predefined target distribution ν , which is given by samples. Finally, we derive a generative model by training a sequence $(\Phi_l)_{l=1}^L$ of neural networks, where each Φ_l approximates a certain number of steps of the particle flow. This allows us to train our network iteratively. In particular, during the training and evaluation procedure, we always consider only one of the networks Φ_l at the same time. This allows an efficient training with relatively low resources even though all networks Φ_l together have a large number of parameters. We demonstrate the efficiency of our generative sliced MMD flows for image generation on MNIST, FashionMNIST and CIFAR10.

Related Work. Approximating gradient flows on measure-spaces for generative modelling was addressed in several papers [2, 3, 21, 22, 23, 30, 52, 55, 58]. However, in all of these papers divergence-based functionals are minimized and it is required to solve an optimization problem in each step. Accelerations of such methods with sliced Wasserstein distances [61] were proposed in [13, 50, 56, 55]. Gradient flows on measure spaces with respect to other metrics are considered in [17, 18, 27, 48, 49] under the name Stein variational gradient descent. Closely related to these gradient flow approximations are score-based and diffusion models [34, 64, 65, 66], which are based on the Langevin dynamics. This can be considered as a gradient flow with respect to the KL divergence. Several combinations of such Langevin-type Markov chain Monte Carlo methods with other generative models were proposed in [5, 9, 29, 76].

Gradient flows with respect to MMD functionals are considered in [1, 4, 32, 42]. However, due to the quadratic complexity of the computation of the derivative of MMD functionals in the number of support points of the involved measures, these papers have a rather theoretical scope and applications are limited to measures supported on a few hundred points. The authors of [42] observe that the sliced MMD is again a MMD functional *with a different kernel*. We use this result in Section 2. In

very low dimensions, fast evaluations of MMD and their gradients were proposed in [26, 73] based on fast Fourier summation using the non-equispaced fast Fourier transforms (NFFT), see [59, Sec. 7] and references therein. Unfortunately, since the complexity of the NFFT depends exponentially on the data-dimension, these approaches are limited to applications in dimension four or smaller.

Finally, the authors of [10, 20, 46, 47] apply MMD for generative modelling by constructing so-called MMD-GANs. However, this is conceptionally a very different approach since in MMD-GANs the discriminator in the classical GAN framework [25] is replaced by a MMD distance with a variable kernel. Similar to GAN ideas this results in a max-min problem which is solved in an alternating fashion and is not related to gradient flows.

Outline of the Paper. In Section 2, we prove that the sliced MMD with the one-dimensional Riesz kernel coincides with MMD of the scaled d -dimensional kernel. This can be used to establish an interesting lower bound on the MMD by the Wasserstein-1 distance. Then, in Section 3 we propose a sorting algorithm for computing the derivative of the sliced MMD in an efficient way. We apply the fast evaluation of MMD gradients to simulate MMD flows and to derive a generative model in Section 4. Section 5 shows numerical experiments on image generation. Finally, conclusions are drawn in Section 6. The appendices contain the proofs and supplementary material.

2 Sliced MMD for Riesz Kernels

Let $\mathcal{P}(\mathbb{R}^d)$ denote the set of probability measures on \mathbb{R}^d and $\mathcal{P}_p(\mathbb{R}^d)$ its subset of measures with finite p -th moment, i.e., $\int_{\mathbb{R}^d} \|x\|^p d\mu(x) < \infty$. Here $\|\cdot\|$ denotes the Euclidean norm on \mathbb{R}^d . For a symmetric, positive definite kernel $K: \mathbb{R}^d \times \mathbb{R}^d \rightarrow \mathbb{R}$, the *maximum mean discrepancy* (MMD) $\mathcal{D}_K: \mathcal{P}(\mathbb{R}^d) \times \mathcal{P}(\mathbb{R}^d) \rightarrow \mathbb{R}$ is the square root of $\mathcal{D}_K^2(\mu, \nu) := \mathcal{E}_K(\mu - \nu)$, where \mathcal{E}_K is the *interaction energy* of signed measures on \mathbb{R}^d defined by

$$\mathcal{E}_K(\eta) := \frac{1}{2} \int_{\mathbb{R}^d} \int_{\mathbb{R}^d} K(x, y) d\eta(x) d\eta(y).$$

Due to its favorable properties, see Appendix E, we are interested in Riesz kernels

$$K(x, y) = -\|x - y\|^r, \quad r \in (0, 2).$$

These kernels are only conditionally positive definite, but can be extended to positive definite kernels by $\tilde{K}(x, y) = K(x, y) - K(x, 0) - K(0, y)$, see also Remark 12. Then it holds $\mathcal{D}_K(\mu, \nu) = \mathcal{D}_{\tilde{K}}(\mu, \nu)$, see [53, Lemma 3.3]. Moreover, for Riesz kernels, \mathcal{D}_K is a metric on $\mathcal{P}_2(\mathbb{R}^d)$, which is also known as so-called energy distance [63, 72] in the literature.

However, computing MMDs on high dimensional spaces is computationally costly. Therefore, the *sliced MMD* $\mathcal{SD}_K^2: \mathcal{P}_2(\mathbb{R}^d) \times \mathcal{P}_2(\mathbb{R}^d) \rightarrow \mathbb{R}$ was considered in the literature, see e.g., [42]. For a symmetric 1D kernel $k: \mathbb{R} \times \mathbb{R} \rightarrow \mathbb{R}$ it is given by

$$\mathcal{SD}_K^2(\mu, \nu) := \mathbb{E}_{\xi \sim \mathcal{U}_{\mathbb{S}^{d-1}}} [\mathcal{D}_k^2(P_{\xi\#}\mu, P_{\xi\#}\nu)]$$

with the push-forward measure $P_{\xi\#}\mu := \mu \circ P_{\xi}^{-1}$ of the projection $P_{\xi}(x) := \langle \xi, x \rangle$ and the uniform distribution $\mathcal{U}_{\mathbb{S}^{d-1}}$ on the sphere \mathbb{S}^{d-1} . By interchanging the integrals from the expectation and the definition of MMD, Kolouri et al. [42] observed that the sliced MMD is equal to the MMD with an associate kernel $K: \mathbb{R}^d \times \mathbb{R}^d \rightarrow \mathbb{R}$. More precisely, it holds

$$\mathcal{SD}_K^2(\mu, \nu) = \mathcal{D}_K^2(\mu, \nu), \quad \text{with } K(x, y) := \mathbb{E}_{\xi \sim \mathcal{U}_{\mathbb{S}^{d-1}}} [k(P_{\xi}(x), P_{\xi}(y))].$$

By the following theorem, this relation becomes more simple when dealing with Riesz kernels, since in this case the associate kernel is a Riesz kernel as well.

Theorem 1 (Sliced Riesz Kernels are Riesz Kernels). *Let $k(x, y) := -|x - y|^r$, $r \in (0, 2)$. Then it holds $\mathcal{SD}_K^2(\mu, \nu) = \mathcal{D}_K^2(\mu, \nu)$ with the associated scaled Riesz kernel*

$$K(x, y) := -c_{d,r}^{-1} \|x - y\|^r, \quad c_{d,r} := \frac{\sqrt{\pi} \Gamma(\frac{d+r}{2})}{\Gamma(\frac{d}{2}) \Gamma(\frac{r+1}{2})}.$$

The proof is given in Appendix A. For $r = 1$, we just write $c_d := c_{d,1}$.

Interestingly, based on Theorem 1, we can establish a relation between the MMD and the Wasserstein-1 distance on $\mathcal{P}_1(\mathbb{R}^d)$ defined by

$$\mathcal{W}_1(\mu, \nu) := \min_{\pi \in \Pi(\mu, \nu)} \int \|x - y\| d\pi(x, y),$$

where $\Pi(\mu, \nu)$ denotes the set of measures in $\mathcal{P}_1(\mathbb{R}^d \times \mathbb{R}^d)$ with marginals μ and ν . The proof is given in Appendix B.

Theorem 2 (Relation between \mathcal{D}_K and \mathcal{W}_1 for Distance Kernels). *Let $K(x, y) := -\|x - y\|$. Then, it holds for $\mu, \nu \in \mathcal{P}(\mathbb{R}^d)$ that*

$$2\mathcal{D}_K^2(\mu, \nu) \leq \mathcal{W}_1(\mu, \nu).$$

If μ and ν are additionally supported on the ball $B_R(0)$, then there exists a constant $C_d > 0$ such that

$$\mathcal{W}_1(\mu, \nu) \leq C_d R^{\frac{2d+1}{2d+2}} \mathcal{D}_K(\mu, \nu)^{\frac{1}{d+1}}.$$

3 Gradients of Sliced MMD

Next, we consider the functional $\mathcal{F}_\nu: \mathcal{P}_2(\mathbb{R}^d) \rightarrow \mathbb{R}$ given by

$$\mathcal{F}_\nu(\mu) := \mathcal{E}_K(\mu) + \mathcal{V}_{K,\nu}(\mu) = \mathcal{D}_K^2(\mu, \nu) + \text{const}_\nu, \quad (2)$$

where $\mathcal{V}_{K,\nu}(\mu)$ is the so-called *potential energy*

$$\mathcal{V}_{K,\nu}(\mu) := - \int_{\mathbb{R}^d} \int_{\mathbb{R}^d} K(x, y) d\nu(y) d\mu(x)$$

acting as an attraction term between the masses of μ and ν , while the interaction energy \mathcal{E}_K is a repulsion term enforcing a proper spread of μ . For the rest of the paper, we always consider the negative distance kernel $K(x, y) := -\|x - y\|$, which is the Riesz kernel (1) with $r = 1$. Then, we obtain directly from the metric property of MMD that the minimizer of the non-convex functional \mathcal{F}_ν is given by ν . We are interested in computing gradient flows of \mathcal{F}_ν towards this minimizer. However, the computation of gradients in measure spaces for discrepancy functionals with non-smooth kernels is highly non-trivial and computationally costly, see e.g., [1, 32].

As a remedy, we focus on a discrete form of the d -dimensional MMD. More precisely, we assume that μ and ν are empirical measures, i.e., they are of the form $\mu = \frac{1}{N} \sum_{i=1}^N \delta_{x_i}$ and $\nu = \frac{1}{M} \sum_{j=1}^M \delta_{y_j}$ for some $x_j, y_j \in \mathbb{R}^d$. Let $\mathbf{x} := (x_1, \dots, x_N)$ and $\mathbf{y} := (y_1, \dots, y_M)$. Then the functional \mathcal{F}_ν reduces to the function $F_d(\cdot|\mathbf{y}): \mathbb{R}^{Nd} \rightarrow \mathbb{R}$ given by

$$\begin{aligned} F_d(\mathbf{x}|\mathbf{y}) &= -\frac{1}{2N^2} \sum_{i=1}^N \sum_{j=1}^N \|x_i - x_j\| + \frac{1}{MN} \sum_{i=1}^N \sum_{j=1}^M \|x_i - y_j\| \\ &= \mathcal{D}_K^2\left(\frac{1}{N} \sum_{i=1}^N \delta_{x_i}, \frac{1}{M} \sum_{j=1}^M \delta_{y_j}\right) + \text{const}_{\mathbf{y}}. \end{aligned} \quad (3)$$

In order to evaluate the gradient of F_d with respect to the support points \mathbf{x} , we use Theorem 1 to rewrite $F_d(\mathbf{x}|\mathbf{y})$ as

$$F_d(\mathbf{x}|\mathbf{y}) = c_d \mathbb{E}_{\xi \sim \mathcal{U}_{\mathbb{S}^{d-1}}} [F_1(\langle \xi, x_1 \rangle, \dots, \langle \xi, x_N \rangle | \langle \xi, y_1 \rangle, \dots, \langle \xi, y_M \rangle)].$$

Then, the gradient of F_d with respect to x_i is given by

$$\nabla_{x_i} F_d(\mathbf{x}|\mathbf{y}) = c_d \mathbb{E}_{\xi \sim \mathcal{U}_{\mathbb{S}^{d-1}}} [\partial_i F_1(\langle \xi, x_1 \rangle, \dots, \langle \xi, x_N \rangle | \langle \xi, y_1 \rangle, \dots, \langle \xi, y_M \rangle) \xi], \quad (4)$$

where $\partial_i F_1$ denotes the derivative of F_1 with respect to the i -th component of the input. Consequently, it suffices to compute gradients of F_1 in order to evaluate the gradient of F_d .

Algorithm 1 Derivative of the interaction energy E from (5).

Input: $x_1, \dots, x_N \in \mathbb{R}$ with $x_i \neq x_j$ for $i \neq j$.

Algorithm:

Compute $\sigma_1, \dots, \sigma_N = \text{argsort}(x_1, \dots, x_N)$.

Compute $g_i = -\frac{2\sigma_i - 1 - N}{N^2}$.

Output: $(g_1, \dots, g_N) = \nabla E(x_1, \dots, x_N)$.

Algorithm 2 Derivative of the potential energy V from (5).

Input: $x_1, \dots, x_N \in \mathbb{R}, y_1, \dots, y_M \in \mathbb{R}$ with $x_i \neq y_j$.

Algorithm:

Compute $\sigma_1, \dots, \sigma_{N+M} = \text{argsort}(x_1, \dots, x_N, y_1, \dots, y_M)$

Initialize $\tilde{h}_1 = \dots = \tilde{h}_{M+N} = 0$.

for $j = 1, \dots, M$ **do**

 Set $\tilde{h}_{\sigma(N+j)} = 1$.

end for

Set $h = 2 \text{cumsum}(\tilde{h}) - 1$

for $i = 1, \dots, N$ **do**

 Set $g_i = \frac{h_{\sigma^{-1}(i)}}{MN}$,

end for

Output: $(g_1, \dots, g_N) = \nabla V(x_1, \dots, x_N | y_1, \dots, y_M)$.

A Sorting Algorithm for the 1D-Case. Next, we derive a sorting algorithm to compute the gradient of F_1 efficiently. In particular, the proposed algorithm has complexity $O((M+N)\log(M+N))$ even though the definition of F_1 in (3) involves $N^2 + MN$ summands.

To this end, we split the functional F_1 into interaction and potential energy, i.e., $F_1(\mathbf{x}|\mathbf{y}) = E(\mathbf{x}) + V(\mathbf{x}|\mathbf{y})$ with

$$E(\mathbf{x}) := -\frac{1}{2N^2} \sum_{i=1}^N \sum_{j=1}^N |x_i - x_j|, \quad V(\mathbf{x}|\mathbf{y}) := \frac{1}{NM} \sum_{i=1}^N \sum_{j=1}^M |x_i - y_j|. \quad (5)$$

Then, we can compute the derivatives of E and V by the following theorem which proof is given in Appendix C.

Theorem 3 (Derivatives of Interaction and Potential Energy). *Let $x_1, \dots, x_N \in \mathbb{R}$ be pairwise disjoint and $y_1, \dots, y_M \in \mathbb{R}$ such that $x_i \neq y_j$ for all $i = 1, \dots, N$ and $j = 1, \dots, M$. Then, E and V are differentiable with*

$$\nabla_{x_i} E(\mathbf{x}) = \frac{N+1-2\sigma(i)}{N^2}, \quad \nabla_{x_i} V(\mathbf{x}|\mathbf{y}) = \frac{2\#\{j \in \{1, \dots, M\} : y_j < x_i\} - M}{MN},$$

where $\sigma: \{1, \dots, N\} \rightarrow \{1, \dots, N\}$ is the permutation with $x_{\sigma(1)} < \dots < x_{\sigma(N)}$.

By Theorem 3, we obtain that $\nabla F_1(\mathbf{x}|\mathbf{y}) = \nabla E(\mathbf{x}) + \nabla V(\mathbf{x}|\mathbf{y})$ can be computed by Algorithm 1 and Algorithm 2 with complexity $O(N \log(N))$ and $O((M+N)\log(M+N))$, respectively. The complexity is dominated by the sorting procedure. Both algorithms can be implemented in a vectorized form for computational efficiency. Note that by Lemma 8 from the appendix, the discrepancy with Riesz kernel and $r = 1$ can be represented by the cumulative distribution functions (cdfs) of the involved measures. Since the cdf of an one-dimensional empirical measure can be computed via sorting, we also obtain an $O((N+M)\log(M+N))$ algorithm for computing the one-dimensional MMD itself and not only for its derivative.

Stochastic Approximation of Sliced MMD Gradients for $r = 1$. To evaluate the gradient of F_d efficiently, we use a stochastic gradient estimator. For $x_1, \dots, x_N, y_1, \dots, y_M \in \mathbb{R}^d$, we define for $P \in \mathbb{N}$ the stochastic gradient estimator of (4) as the random variable

$$\tilde{\nabla}_P F_d(\mathbf{x}|\mathbf{y}) = \left(\tilde{\nabla}_{P, x_i} F_d(\mathbf{x}|\mathbf{y}) \right)_{i=1}^N \quad (6)$$

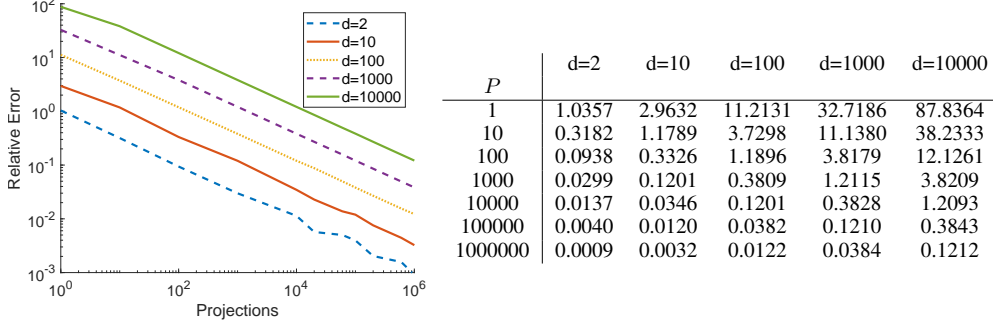


Figure 1: Relative error of the gradients of sliced MMD and MMD with respect to the number of projections and dimensions. The results show the relative error decays in $O(\frac{1}{\sqrt{P}})$ as shown in Theorem 4.

where

$$\tilde{\nabla}_{P, x_i} F_d(\mathbf{x}|\mathbf{y}) := \frac{c_d}{P} \sum_{p=1}^P \partial_i F_1(\langle \xi_p, x_1 \rangle, \dots, \langle \xi_p, x_N \rangle | \langle \xi_p, y_1 \rangle, \dots, \langle \xi_p, y_M \rangle) \xi_p,$$

for independent random variables $\xi_1, \dots, \xi_P \sim \mathcal{U}_{\mathbb{S}^{d-1}}$. We obtain by (4) that $\tilde{\nabla} F_d$ is unbiased, i.e.,

$$\mathbb{E}[\tilde{\nabla}_P F_d(\mathbf{x}|\mathbf{y})] = \nabla F_d(\mathbf{x}|\mathbf{y}).$$

Moreover, the following theorem shows that the error of $\tilde{\nabla}_P F_d$ converges to zero for a growing number P of projections. The proof uses classical concentration inequalities and follows directly from Corollary 11 in Appendix D.

Theorem 4 (Error Bound for Stochastic MMD Gradients). *Let $x_1, \dots, x_N, y_1, \dots, y_M \in \mathbb{R}^d$. Then, it holds*

$$\mathbb{E}[||\tilde{\nabla}_P F_d(\mathbf{x}|\mathbf{y}) - \nabla F_d(\mathbf{x}|\mathbf{y})||] \in O\left(\sqrt{\frac{d}{P}}\right).$$

To verify this convergence rate numerically, we draw $N = 1000$ samples x_1, \dots, x_N from a Gaussian mixture model with two components and $M = 1000$ samples y_1, \dots, y_M from a Gaussian mixture model with ten components. The means are chosen randomly following a uniform distribution in $[-1, 1]^d$ and the standard deviation is set to 0.01. Then, we compute numerically the expected relative approximation error between $\tilde{\nabla}_P F_d$ and ∇F_d for different choices of P and d . The results are illustrated in Figure 1. We observe that this numerical evaluation underlines the convergence rate of $O\left(\sqrt{\frac{d}{P}}\right)$. In particular, the error scales with $O(\sqrt{d/P})$, which makes the approach applicable for high-dimensional problems.

Remark 5 (Computational Complexity of Gradient Evaluations). *By Theorem 4, we require $O(d)$ projections in order to approximate $\nabla F_d(\mathbf{x}|\mathbf{y})$ by $\tilde{\nabla}_P F_d(\mathbf{x}|\mathbf{y})$ up to a fixed expected error of ϵ . Together with the computational complexity of $O(dP(N + M) \log(N + M))$ for $\tilde{\nabla}_P F_d(\mathbf{x}, \mathbf{y})$, we obtain an overall complexity of $O(d^2(N + M) \log(N + M))$ in order to approximate $\nabla F_d(\mathbf{x}|\mathbf{y})$ up to an expected error of ϵ . On the other hand, the naive computation of (gradients of) $F_d(\mathbf{x}|\mathbf{y})$ has a complexity of $O(d(N^2 + MN))$. Consequently, we improve the quadratic complexity in the number of samples to $O(N \log(N))$. Here, we pay the price of quadratic instead of linear complexity in the dimension.*

4 Generative MMD Flows

In this section, we use MMD flows with the negative distance kernel for generative modelling. Throughout this section, we assume that we are given independent samples $y_1, \dots, y_M \in \mathbb{R}^d$ from a target measure $\nu \in \mathcal{P}_2(\mathbb{R}^d)$ and define the empirical version of ν by $\nu_M := \frac{1}{M} \sum_{i=1}^M \delta_{y_i}$.

4.1 MMD Particle Flows

In order to derive a generative model approximating ν , we simulate a gradient flow of the functional \mathcal{F}_ν from (2). Unfortunately, the computation of gradient flows in measure spaces for \mathcal{F}_ν is highly non-trivial and computationally costly, see [1, 32]. Therefore, we consider the (rescaled) gradient flow with respect to the functional F_d instead. More precisely, we simulate for F_d from (3), the (Euclidean) differential equation

$$\dot{x} = -N \nabla F_d(\mathbf{x}|\mathbf{y}), \quad x(0) = (x_1^{(0)}, \dots, x_N^{(0)}), \quad (7)$$

where the initial points $x_i^{(0)}$ are drawn independently from some measure $\mu_0 \in \mathcal{P}_2(\mathbb{R}^d)$. In our numerical experiments, we set μ_0 to the uniform distribution on $[0, 1]^d$. Then, for any solution $x(t) = (x_1(t), \dots, x_N(t))$ of (7), it is proven in [1, Proposition 14] that the curve $\gamma_{M,N}: (0, \infty) \rightarrow \mathcal{P}_2(\mathbb{R}^d)$ defined by $\gamma_{M,N}(t) = \frac{1}{N} \sum_{i=1}^N \delta_{x_i(t)}$ is a Wasserstein gradient flow with respect to the function

$$\mathcal{F}: \mathcal{P}_2(\mathbb{R}^d) \rightarrow \mathbb{R} \cup \{\infty\}, \quad \mu \mapsto \begin{cases} \mathcal{F}_{\nu_M}, & \text{if } \mu = \frac{1}{N} \sum_{i=1}^N \delta_{x_i} \text{ for some } x_i \neq x_j \in \mathbb{R}^d, \\ +\infty, & \text{otherwise.} \end{cases}$$

Hence, we can expect for $M, N \rightarrow \infty$, that the curve $\gamma_{M,N}$ approximates the Wasserstein gradient flow with respect to \mathcal{F}_ν . Consequently, we can derive a generative model by simulating the gradient flow (7). To this end, we use the explicit Euler scheme

$$\mathbf{x}^{(k+1)} = \mathbf{x}^{(k)} - \tau N \nabla F_d(\mathbf{x}^{(k)}|\mathbf{y}), \quad (8)$$

where $\mathbf{x}^{(k)} = (x_1^{(k)}, \dots, x_N^{(k)})$ and $\tau > 0$ is some step size. Here, the gradient on the right-hand side can be evaluated very efficiently by the stochastic gradient estimator from (6).

Momentum MMD Flows. To reduce the required number of steps in (8), we introduce a momentum parameter. More precisely, for some given momentum parameter $m \in [0, 1)$ we consider the momentum MMD flow defined by the following iteration

$$\begin{aligned} \mathbf{v}^{(k+1)} &= \nabla F_d(\mathbf{x}^{(k)}|\mathbf{y}) + m \mathbf{v}^{(k)} \\ \mathbf{x}^{(k+1)} &= \mathbf{x}^{(k)} - \tau N \mathbf{v}^{(k+1)}, \end{aligned} \quad (9)$$

where $\tau > 0$ is some step size, $x_i^{(0)}$ are independent samples from a initial measure μ_0 and $v_i^{(0)} = 0$. Note that the MMD flow (8) is a special case of the momentum MMD flow (9) with $m = 0$.

In Figure 2, we illustrate the momentum MMD flow (9) and MMD flow (8) without momentum from a uniform distribution on $[0, 1]^d$ to MNIST [45] and CIFAR10 [44]. The momentum is set to $m = 0.9$ for MNIST and to $m = 0.6$ for CIFAR10. We observe that the momentum MMD flow (9) converges indeed faster than the MMD flow (8) without momentum.

4.2 Generative MMD Flows

The (momentum) MMD flows from (8) and (9) transform samples from the initial distribution μ_0 into samples from the target distribution ν . Therefore, we propose to train a generative model which approximates these schemes. To this end, we iteratively train neural networks Φ_1, \dots, Φ_L , where each of the networks approximates T_l number of steps from (8) or (9). More precisely, we train Φ_1, \dots, Φ_L by Algorithm 3. In the experiments, we choose the loss function ℓ as the mean squared error.

Once the networks Φ_1, \dots, Φ_L are trained, we can infer a new sample x from our (approximated) target distribution ν as follows. We draw a sample $x^{(0)}$ from μ_0 , compute $x^{(l)} = x^{(l-1)} - \Phi_l(x^{(l-1)})$ for $l = 1, \dots, L$ and set $x = x^{(L)}$. In particular, this allows us to simulate paths of the discrepancy flow we have not trained on.

Remark 6 (Iterative Training and Sampling). *Since the networks are not trained in an end-to-end fashion but separately, their GPU memory load is relatively low despite a high number of trainable parameters of the full model $(\Phi_l)_{l=1}^L$. This enables training of our model on an 8 GB GPU. Moreover, the training can easily be continued by adding additional networks Φ_l , $l = L+1, \dots, L'$ to an already trained generative MMD flow $(\Phi_l)_{l=1}^L$, which makes applications more flexible.*

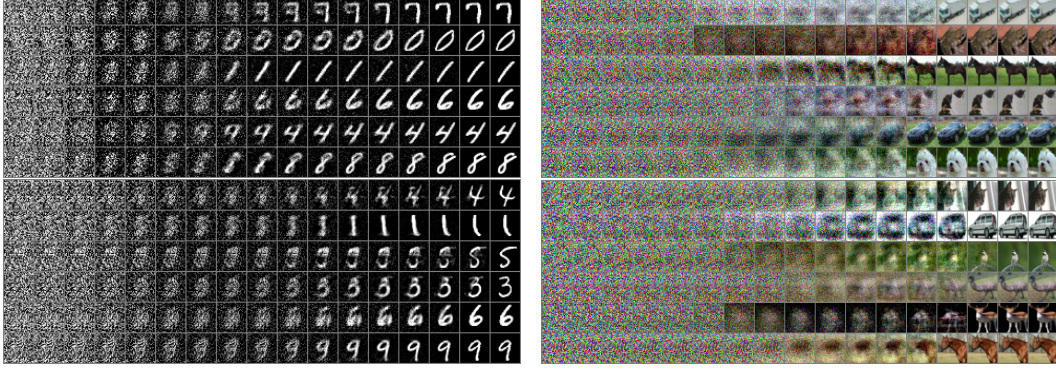


Figure 2: Samples and their trajectories from MNIST (left) and CIFAR10 (right) in the MMD flow with momentum (9, top) and without momentum (8, bottom) starting in the uniform distribution on $[0, 1]^d$ after 2^k steps with $k \in \{0, \dots, 16\}$ (for MNIST) and $k \in \{3, \dots, 19\}$ (for CIFAR10). We observe that the momentum MMD flow (9) converges faster than the MMD flow (8) without momentum.

Algorithm 3 Training of generative MMD flows

Input: Independent initial samples $x_1^{(0)}, \dots, x_N^{(0)}$ from μ_0 , momentum parameters $m_l \in [0, 1)$ for $l = 1, \dots, L$.

Initialize $(v_1, \dots, v_N) = 0$.

for $l = 1, \dots, L$ **do**

- Set $(\tilde{x}_1^{(0)}, \dots, \tilde{x}_N^{(0)}) = (x_1^{(l-1)}, \dots, x_N^{(l-1)})$.
- Simulate T_l steps of the (momentum) MMD flow:

for $t = 1, \dots, T_l$ **do**

- Update v by

$$(v_1, \dots, v_N) \leftarrow \nabla F_d(\tilde{x}_1^{(t-1)}, \dots, \tilde{x}_N^{(t-1)} | y_1, \dots, y_M) + m_l(v_1, \dots, v_N)$$

- Update the flow samples:

$$(\tilde{x}_1^{(t)}, \dots, \tilde{x}_N^{(t)}) = (\tilde{x}_1^{(t-1)}, \dots, \tilde{x}_N^{(t-1)}) - \tau N(v_1, \dots, v_N)$$

end for

- Train Φ_l such that $\tilde{x}^{(T_l)} \approx \tilde{x}^{(0)} - \Phi_l(\tilde{x}^{(0)})$ by minimizing the loss

$$\mathcal{L}(\theta_l) = \frac{1}{N} \sum_{i=1}^N \ell(\Phi_l(\tilde{x}_i^{(0)}), (\tilde{x}_i^{(0)} - \tilde{x}_i^{(T_l)}))$$

for some $\ell: \mathbb{R}^d \times \mathbb{R}^d \rightarrow \mathbb{R}$.

- Set $(x_1^{(l)}, \dots, x_N^{(l)}) = (\Phi_l(x_1^{(l-1)}), \dots, \Phi_l(x_N^{(l-1)}))$.

end for

5 Numerical Examples

In this section, we apply generative MMD flows for image generation on MNIST, FashionMNIST [77] and CIFAR10. The images from MNIST and FashionMNIST are 28×28 gray-value images, while CIFAR10 consists of 32×32 RGB images resulting in the dimensions $d = 784$ and $d = 3072$, respectively. We run all experiments on a single NVIDIA GeForce RTX 2060 Super GPU with 8GB memory. To evaluate our results, we use the Fréchet inception distance (FID) [33]¹ between 10K generated samples and the test dataset. Here, a smaller FID value indicates a higher similarity between generated and test samples.

¹We use the implementation from <https://github.com/mseitzer/pytorch-fid>.

Table 1: FID scores for different datasets and various methods.

Method	MNIST	FashionMNIST	CIFAR10
<i>Auto-encoder based</i>			
SWAE [43] ⁴	29.8	74.3	141.9
CWAE [40]	23.6	50.0	120.0
SWF+ Autoencoder + RealNVP [13]	17.8	40.6	-
2-stage VAE [16]	12.6	29.3	72.9
GLF [78]	8.2	21.3	88.3
<i>Adversarial</i>			
WGAN [7, 51]	6.7	21.5	-
MMD GAN [10]	4.2	-	48.1
<i>Score-based</i>			
NCSN [64]	-	-	25.3
<i>Flow based</i>			
SWF [50] ³	225.1	207.6	-
SIG [15]	4.5	13.7	66.5
Generative Sliced MMD Flow (ours)	3.1	11.4	67.2

We choose the networks $(\Phi_l)_{l=1}^L$ to be UNets [62], where we use the implementation from [35] based on [34]. The number P of projections is chosen by $P = 1000$ for MNIST and FashionMNIST and by $P = 4000$ for CIFAR10. Then, we run the generative MMD flow for $L = 55$ (MNIST), $L = 67$ (FashionMNIST) and $L = 55$ (CIFAR10) networks. The exact setup is described in Appendix G. We compare the resulting FIDs with other gradient-flow-based models and various further methods in Table 1. We observe that we achieve excellent performance on MNIST and FashionMNIST as well as first promising results on CIFAR10. Samples from the original dataset as well as generated samples are given in Figure 3.

In Figure 4, we compare generated MNIST samples with the closest samples from the training set. We observe that they are significantly different. Hence, our method generates really new samples and is not just reproducing the samples from the training set.

³values taken from [13]

⁴values taken from [15]



Figure 3: Test set samples (top) and generated samples (bottom) of our generative MMD Flow.



Figure 4: Generated samples (top), closest samples from the training set (middle) and the pixelwise distance between them (bottom). The mean PSNR between these generated images and the corresponding closest training images is 16.94.

6 Conclusions

Evaluating the MMD and its gradient suffers from intractable computational costs, especially if the number of support points of the involved measures becomes large. For Riesz kernels we showed that the MMD coincides with a sliced version of MMD such that we can reduce the problem to the one-dimensional setting. Here we can use an efficient sorting algorithm to compute gradients of the MMD functional. For the implementations, we approximated the gradient of sliced MMD by a finite number of slices and proved that the corresponding approximation error depends by a square root on the dimension. Thus, this technique allows for the application of MMD flows even for applications such as image generation on MNIST, FashionMNIST and CIFAR10.

One of the disadvantages of interacting particle methods is that batching is not easily possible: The particle flow for one set of training points does not give a helpful approximation for another set of training points. This is due to the interaction energy and a general problem of particle flows. Furthermore, taking the projections involves multiplication of every data point with a "full" projection and therefore scales with the dimension d . Taking "local" projections like in [19, 54] can be much more efficient.

Our paper is the first work which utilizes sliced MMD flows for generative modelling. Consequently the approach can be extended in several directions. From a theoretical viewpoint, the derivative formulas from Theorem 3 can be extended to the non-discrete case by the use of quantile functions, see [11, 31] for some first approaches into this direction. Towards applications, we could extend the framework to posterior sampling in Bayesian inverse problems. In this context, the fast computation of MMD gradients can be also of interest for applications which are not based on gradient flows, e.g., [6]. Finally, the consideration of sliced probability metrics is closely related to the Radon transform and is therefore of interest also for non-Euclidean domains like the sphere, see e.g., [12, 60].

Acknowledgement

Many thanks to J. Chemseddine for providing parts of the proof of Theorem 2, and to R. Beinert and G. Steidl for fruitful discussions.

J.H. acknowledges funding by the German Research Foundation (DFG) within the project STE 571/16-1, C.W. by the DFG within the SFB "Tomography Across the Scales" (STE 571/19-1, project number: 495365311), F.A. by the DFG under Germany's Excellence Strategy – The Berlin Mathematics Research Center MATH+ (project TP: EF3-7), and P.H. from the DFG within the project SPP 2298 "Theoretical Foundations of Deep Learning".

References

- [1] F. Altekruiger, J. Hertrich, and G. Steidl. Neural Wasserstein gradient flows for maximum mean discrepancies with Riesz kernels. In *Proceedings of the 40th International Conference on Machine Learning*, volume 202 of *Proceedings of Machine Learning Research*, pages 664–690. PMLR, 2023.
- [2] D. Alvarez-Melis, Y. Schiff, and Y. Mroueh. Optimizing functionals on the space of probabilities with input convex neural networks. *Transactions on Machine Learning Research*, 2022.
- [3] A. F. Ansari, M. L. Ang, and H. Soh. Refining deep generative models via discriminator gradient flow. In *International Conference on Learning Representations*, 2021.

- [4] M. Arbel, A. Korba, A. Salim, and A. Gretton. Maximum mean discrepancy gradient flow. In H. Wallach, H. Larochelle, A. Beygelzimer, F. d'Alché-Buc, E. Fox, and R. Garnett, editors, *Advances in Neural Information Processing Systems*, volume 32. Curran Associates, Inc., 2019.
- [5] M. Arbel, A. Matthews, and A. Doucet. Annealed flow transport monte carlo. In *International Conference on Machine Learning*. PMLR, 2021.
- [6] L. Ardizzone, J. Kruse, C. Rother, and U. Köthe. Analyzing inverse problems with invertible neural networks. In *International Conference on Learning Representations*, 2019.
- [7] M. Arjovsky, S. Chintala, and L. Bottou. Wasserstein generative adversarial networks. In *International Conference on Machine Learning*, 2017.
- [8] K. Atkinson and W. Han. *Spherical harmonics and approximations on the unit sphere: an introduction*, volume 2044. Springer Science & Business Media, 2012.
- [9] H. Ben-Hamu, S. Cohen, J. Bose, B. Amos, M. Nickel, A. Grover, R. T. Q. Chen, and Y. Lipman. Matching normalizing flows and probability paths on manifolds. In K. Chaudhuri, S. Jegelka, L. Song, C. Szepesvari, G. Niu, and S. Sabato, editors, *Proceedings of the 39th International Conference on Machine Learning*, volume 162 of *Proceedings of Machine Learning Research*, pages 1749–1763. PMLR, 2022.
- [10] M. Bińkowski, D. J. Sutherland, M. Arbel, and A. Gretton. Demystifying MMD GANs. In *International Conference on Learning Representations*, 2018.
- [11] G. A. Bonaschi, J. A. Carrillo, M. Di Francesco, and M. A. Peletier. Equivalence of gradient flows and entropy solutions for singular nonlocal interaction equations in 1D. *ESAIM: Control, Optimisation and Calculus of Variations*, 21(2):414–441, 2015.
- [12] C. Bonet, P. Berg, N. Courty, F. Septier, L. Drumetz, and M.-T. Pham. Spherical sliced-wasserstein. *arXiv preprint arXiv:2206.08780*, 2022.
- [13] C. Bonet, N. Courty, F. Septier, and L. Drumetz. Efficient gradient flows in sliced-Wasserstein space. *Transactions on Machine Learning Research*, 2022.
- [14] N. Bonnotte. Unidimensional and evolution methods for optimal transportation. *PhD Thesis, Univ. Paris-Sud*, 2013.
- [15] B. Dai and U. Seljak. Sliced iterative normalizing flows. In M. Meila and T. Zhang, editors, *Proceedings of the 38th International Conference on Machine Learning*, volume 139 of *Proceedings of Machine Learning Research*, pages 2352–2364. PMLR, 2021.
- [16] B. Dai and D. Wipf. Diagnosing and enhancing VAE models. In *International Conference on Learning Representations*, 2019.
- [17] L. L. di Langosco, V. Fortuin, and H. Strathmann. Neural variational gradient descent. In *Fourth Symposium on Advances in Approximate Bayesian Inference*, 2022.
- [18] H. Dong, X. Wang, L. Yong, and T. Zhang. Particle-based variational inference with pre-conditioned functional gradient flow. In *The Eleventh International Conference on Learning Representations*, 2023.
- [19] C. Du, T. Li, T. Pang, S. Yan, and M. Lin. Nonparametric generative modeling with conditional sliced-Wasserstein flows. In A. Krause, E. Brunskill, K. Cho, B. Engelhardt, S. Sabato, and J. Scarlett, editors, *Proceedings of the 40th International Conference on Machine Learning*, volume 202 of *Proceedings of Machine Learning Research*, pages 8565–8584. PMLR, 23–29 Jul 2023.
- [20] G. K. Dziugaite, D. M. Roy, and Z. Ghahramani. Training generative neural networks via maximum mean discrepancy optimization. In *Proceedings of the Thirty-First Conference on Uncertainty in Artificial Intelligence*, pages 258–267, 2015.
- [21] J. Fan, Q. Zhang, A. Taghvaei, and Y. Chen. Variational Wasserstein gradient flow. In K. Chaudhuri, S. Jegelka, L. Song, C. Szepesvari, G. Niu, and S. Sabato, editors, *Proceedings of the 39th International Conference on Machine Learning*, volume 162 of *Proceedings of Machine Learning Research*, pages 6185–6215. PMLR, 2022.
- [22] Y. Gao, Y. Jiao, Y. Wang, Y. Wang, C. Yang, and S. Zhang. Deep generative learning via variational gradient flow. In K. Chaudhuri and R. Salakhutdinov, editors, *Proceedings of the 36th International Conference on Machine Learning*, volume 97 of *Proceedings of Machine Learning Research*, pages 2093–2101. PMLR, 2019.

- [23] N. Garcia Trillos, B. Hosseini, and D. Sanz-Alonso. From optimization to sampling through gradient flows. *arXiv preprint arXiv:2302.11449*, 2023.
- [24] P. Glaser, M. Arbel, and A. Gretton. KALE Flow: A relaxed KL gradient flow for probabilities with disjoint support. In M. Ranzato, A. Beygelzimer, Y. Dauphin, P. Liang, and J. W. Vaughan, editors, *Advances in Neural Information Processing Systems*, volume 34, pages 8018–8031. Curran Associates, Inc., 2021.
- [25] I. Goodfellow, J. Pouget-Abadie, M. Mirza, B. Xu, D. Warde-Farley, S. Ozair, A. Courville, and Y. Bengio. Generative adversarial nets. In Z. Ghahramani, M. Welling, C. Cortes, N. Lawrence, and K. Weinberger, editors, *Advances in Neural Information Processing Systems*, volume 27. Curran Associates, Inc., 2014.
- [26] M. Gräf, D. Potts, and G. Steidl. Quadrature errors, discrepancies, and their relations to halftoning on the torus and the sphere. *SIAM Journal on Scientific Computing*, 34(5):A2760–A2791, 2012.
- [27] W. Grathwohl, K.-C. Wang, J.-H. Jacobsen, D. K. Duvenaud, and R. S. Zemel. Learning the stein discrepancy for training and evaluating energy-based models without sampling. In *International Conference on Machine Learning*, 2020.
- [28] A. Gretton, K. M. Borgwardt, M. J. Rasch, B. Schölkopf, and A. Smola. A kernel two-sample test. *The Journal of Machine Learning Research*, 13(1):723–773, 2012.
- [29] P. L. Hagemann, J. Hertrich, and G. Steidl. *Generalized normalizing flows via Markov chains*. Cambridge University Press, 2023.
- [30] A. Heng, A. F. Ansari, and H. Soh. Deep generative Wasserstein gradient flows. *Preprint on OpenReview: <https://openreview.net/forum?id=zjSeBTedXp1>*, 2023.
- [31] J. Hertrich, R. Beinert, M. Gräf, and G. Steidl. Wasserstein gradient flows of the discrepancy with distance kernel on the line. In *Scale Space and Variational Methods in Computer Vision*, pages 431–443. Springer, 2023.
- [32] J. Hertrich, M. Gräf, R. Beinert, and G. Steidl. Wasserstein steepest descent flows of discrepancies with Riesz kernels. *arXiv preprint arXiv:2211.01804*, 2023.
- [33] M. Heusel, H. Ramsauer, T. Unterthiner, B. Nessler, and S. Hochreiter. GANs trained by a two time-scale update rule converge to a local nash equilibrium. In I. Guyon, U. V. Luxburg, S. Bengio, H. Wallach, R. Fergus, S. Vishwanathan, and R. Garnett, editors, *Advances in Neural Information Processing Systems*, volume 30. Curran Associates, Inc., 2017.
- [34] J. Ho, A. Jain, and P. Abbeel. Denoising diffusion probabilistic models. In H. Larochelle, M. Ranzato, R. Hadsell, M. Balcan, and H. Lin, editors, *Advances in Neural Information Processing Systems*, volume 33, pages 6840–6851. Curran Associates, Inc., 2020.
- [35] C.-W. Huang, J. H. Lim, and A. Courville. A variational perspective on diffusion-based generative models and score matching. In A. Beygelzimer, Y. Dauphin, P. Liang, and J. W. Vaughan, editors, *Advances in Neural Information Processing Systems*, 2021.
- [36] R. Jordan, D. Kinderlehrer, and F. Otto. The variational formulation of the Fokker–Planck equation. *SIAM Journal on Mathematical Analysis*, 29(1):1–17, 1998.
- [37] D. Kershaw. Some extensions of W. Gautschi’s inequalities for the Gamma function. *Mathematics of Computation*, 41(164):607–611, 1983.
- [38] D. P. Kingma and J. Ba. Adam: A method for stochastic optimization. In *International Conference on Learning Representations*, 2015.
- [39] D. P. Kingma and M. Welling. Auto-encoding variational bayes. In *International Conference on Learning Representations*, 2014.
- [40] S. Knop, P. Spurek, J. Tabor, I. Podolak, M. Mazur, and S. Jastrzębski. Cramer-wold auto-encoder. *Journal of Machine Learning Research*, 21(164):1–28, 2020.
- [41] J. M. Kohler and A. Lucchi. Sub-sampled cubic regularization for non-convex optimization. In *International Conference on Machine Learning*, pages 1895–1904. PMLR, 2017.
- [42] S. Kolouri, K. Nadjahi, S. Shahrampour, and U. Şimşekli. Generalized sliced probability metrics. In *IEEE International Conference on Acoustics, Speech and Signal Processing*, pages 4513–4517, 2022.

- [43] S. Kolouri, P. E. Pope, C. E. Martin, and G. K. Rohde. Sliced wasserstein auto-encoders. In *International Conference on Learning Representations*, 2019.
- [44] A. Krizhevsky. Learning multiple layers of features from tiny images. Master’s thesis, University Toronto, ON, Canada, 2009.
- [45] Y. LeCun, L. Bottou, Y. Bengio, and P. Haffner. Gradient-based learning applied to document recognition. *Proceedings of the IEEE*, 86(11):2278–2324, 1998.
- [46] C.-L. Li, W.-C. Chang, Y. Cheng, Y. Yang, and B. Poczos. MMD GAN: Towards deeper understanding of moment matching network. In I. Guyon, U. V. Luxburg, S. Bengio, H. Wallach, R. Fergus, S. Vishwanathan, and R. Garnett, editors, *Advances in Neural Information Processing Systems*, volume 30. Curran Associates, Inc., 2017.
- [47] Y. Li, K. Swersky, and R. Zemel. Generative moment matching networks. In *International conference on machine learning*, pages 1718–1727. PMLR, 2015.
- [48] Q. Liu. Stein variational gradient descent as gradient flow. In I. Guyon, U. V. Luxburg, S. Bengio, H. Wallach, R. Fergus, S. Vishwanathan, and R. Garnett, editors, *Advances in Neural Information Processing Systems*, volume 30. Curran Associates, Inc., 2017.
- [49] Q. Liu and D. Wang. Stein variational gradient descent: A general purpose Bayesian inference algorithm. In D. Lee, M. Sugiyama, U. Luxburg, I. Guyon, and R. Garnett, editors, *Advances in Neural Information Processing Systems*, volume 29. Curran Associates, Inc., 2016.
- [50] A. Liutkus, U. Simsekli, S. Majewski, A. Durmus, and F.-R. Stöter. Sliced-Wasserstein flows: Nonparametric generative modeling via optimal transport and diffusions. In K. Chaudhuri and R. Salakhutdinov, editors, *Proceedings of the 36th International Conference on Machine Learning*, volume 97 of *Proceedings of Machine Learning Research*, pages 4104–4113. PMLR, 2019.
- [51] M. Lucic, K. Kurach, M. Michalski, S. Gelly, and O. Bousquet. Are GANs created equal? a large-scale study. In S. Bengio, H. Wallach, H. Larochelle, K. Grauman, N. Cesa-Bianchi, and R. Garnett, editors, *Advances in Neural Information Processing Systems*, volume 31. Curran Associates, Inc., 2018.
- [52] P. Mokrov, A. Korotin, L. Li, A. Genevay, J. M. Solomon, and E. Burnaev. Large-scale Wasserstein gradient flows. In M. Ranzato, A. Beygelzimer, Y. Dauphin, P. Liang, and J. W. Vaughan, editors, *Advances in Neural Information Processing Systems*, volume 34, pages 15243–15256, 2021.
- [53] S. Neumayer and G. Steidl. From optimal transport to discrepancy. *Handbook of Mathematical Models and Algorithms in Computer Vision and Imaging: Mathematical Imaging and Vision*, pages 1–36, 2021.
- [54] K. Nguyen and N. Ho. Revisiting sliced Wasserstein on images: From vectorization to convolution. In A. H. Oh, A. Agarwal, D. Belgrave, and K. Cho, editors, *Advances in Neural Information Processing Systems*, 2022.
- [55] K. Nguyen, N. Ho, T. Pham, and H. Bui. Distributional sliced-Wasserstein and applications to generative modeling. In *International Conference on Learning Representations*, 2021.
- [56] K. Nguyen, T. Ren, H. Nguyen, L. Rout, T. M. Nguyen, and N. Ho. Hierarchical sliced Wasserstein distance. In *The Eleventh International Conference on Learning Representations*, 2023.
- [57] E. Novak and H. Wozniakowski. *Tractability of Multivariate Problems. Volume II*, volume 12 of *EMS Tracts in Mathematics*. EMS Publishing House, Zürich, 2010.
- [58] G. Peyré. Entropic approximation of Wasserstein gradient flows. *SIAM Journal on Imaging Sciences*, 8(4):2323–2351, 2015.
- [59] G. Plonka, D. Potts, G. Steidl, and M. Tasche. *Numerical Fourier Analysis*. Springer, 2018.
- [60] M. Quellmalz, R. Beinert, and G. Steidl. Sliced optimal transport on the sphere. *arXiv preprint arXiv:2304.09092*, 2023.
- [61] J. Rabin, G. Peyré, J. Delon, and M. Bernot. Wasserstein barycenter and its application to texture mixing. In *Scale Space and Variational Methods in Computer Vision*, pages 435–446. Springer, 2012.

- [62] O. Ronneberger, P. Fischer, and T. Brox. U-Net: Convolutional networks for biomedical image segmentation. In *Medical Image Computing and Computer-Assisted Intervention*, pages 234–241. Springer, 2015.
- [63] D. Sejdinovic, B. Sriperumbudur, A. Gretton, and K. Fukumizu. Equivalence of distance-based and RKHS-based statistics in hypothesis testing. *The Annals of Statistics*, 41(5):2263 – 2291, 2013.
- [64] Y. Song and S. Ermon. Generative modeling by estimating gradients of the data distribution. In H. Wallach, H. Larochelle, A. Beygelzimer, F. d'Alché-Buc, E. Fox, and R. Garnett, editors, *Advances in Neural Information Processing Systems*, volume 32. Curran Associates, Inc., 2019.
- [65] Y. Song and S. Ermon. Improved techniques for training score-based generative models. In H. Larochelle, M. Ranzato, R. Hadsell, M. Balcan, and H. Lin, editors, *Advances in Neural Information Processing Systems*, volume 33, pages 12438–12448. Curran Associates, Inc., 2020.
- [66] Y. Song, J. Sohl-Dickstein, D. P. Kingma, A. Kumar, S. Ermon, and B. Poole. Score-based generative modeling through stochastic differential equations. In *International Conference on Learning Representations*, 2021.
- [67] B. K. Sriperumbudur, K. Fukumizu, and G. R. Lanckriet. Universality, characteristic kernels and RKHS embedding of measures. *Journal of Machine Learning Research*, 12(7), 2011.
- [68] B. K. Sriperumbudur, A. Gretton, K. Fukumizu, B. Schölkopf, and G. R. Lanckriet. Hilbert space embeddings and metrics on probability measures. *The Journal of Machine Learning Research*, 11:1517–1561, 2010.
- [69] B. K. Sriperumbudur, A. Gretton, K. Fukumizu, B. Schölkopf, and G. R. G. Lanckriet. Hilbert space embeddings and metrics on probability measures, 2010.
- [70] I. Steinwart and A. Christmann. *Support vector machines*. Springer Science & Business Media, 2008.
- [71] G. Székely. E-statistics: The energy of statistical samples. *Techical Report, Bowling Green University*, 2002.
- [72] G. J. Székely and M. L. Rizzo. Energy statistics: A class of statistics based on distances. *Journal of Statistical Planning and Inference*, 143(8):1249–1272, 2013.
- [73] T. Teuber, G. Steidl, P. Gwosdek, C. Schmaltz, and J. Weickert. Dithering by differences of convex functions. *SIAM Journal on Imaging Sciences*, 4(1):79–108, 2011.
- [74] R. Vershynin. *High-dimensional probability: An introduction with applications in data science*, volume 47. Cambridge university press, 2018.
- [75] M. Welling and Y. W. Teh. Bayesian learning via stochastic gradient Langevin dynamics. In *Proceedings of the 28th International Conference on Machine Learning*, pages 681–688, 2011.
- [76] H. Wu, J. Köhler, and F. Noe. Stochastic normalizing flows. In H. Larochelle, M. Ranzato, R. Hadsell, M. Balcan, and H. Lin, editors, *Advances in Neural Information Processing Systems*, volume 33, pages 5933–5944. Curran Associates, Inc., 2020.
- [77] H. Xiao, K. Rasul, and R. Vollgraf. Fashion-MNIST: a novel image dataset for benchmarking machine learning algorithms. *arXiv preprint arXiv:1708.07747*, 2017.
- [78] Z. Xiao, Q. Yan, and Y. Amit. Generative latent flow. *arXiv preprint arXiv:1905.10485*, 2019.

A Proof of Theorem 1

Let $\mathcal{U}_{\mathbb{S}^{d-1}}$ be the uniform distribution on \mathbb{S}^{d-1} and let $k(x, y) = -|x - y|^r$ for $x, y \in \mathbb{R}, x \neq y$ and $r \in (0, 2)$. Moreover, denote by $e = (1, \dots, 0) \in \mathbb{S}^{d-1}$ the first unit vector. Then, we have for $x, y \in \mathbb{R}^d$ that

$$\begin{aligned} K(x, y) &:= - \int_{\mathbb{S}^{d-1}} |\langle \xi, x \rangle - \langle \xi, y \rangle|^r d\mathcal{U}_{\mathbb{S}^{d-1}}(\xi) = -\|x - y\|^r \int_{\mathbb{S}^{d-1}} \left| \left\langle \xi, \frac{x - y}{\|x - y\|} \right\rangle \right|^r d\mathcal{U}_{\mathbb{S}^{d-1}}(\xi) \\ &= -\|x - y\|^r \int_{\mathbb{S}^{d-1}} |\langle \xi, e \rangle|^r d\mathcal{U}_{\mathbb{S}^{d-1}}(\xi) = -\|x - y\|^r \underbrace{\int_{\mathbb{S}^{d-1}} |\xi_1|^r d\mathcal{U}_{\mathbb{S}^{d-1}}(\xi)}_{=: c_{d,r}^{-1}}. \end{aligned}$$

It remains to compute the constant $c_{d,r}$ which is straightforward for $d = 1$. For $d > 1$ the map

$$(t, \eta) \mapsto (t, \eta \sqrt{1 - t^2})$$

defined on $[-1, 1] \times \mathbb{S}^{d-2}$ is a parametrization of \mathbb{S}^{d-1} . The surface measure on \mathbb{S}^{d-1} is then given by

$$d\sigma_{\mathbb{S}^{d-1}}(\xi) = (1 - t^2)^{\frac{d-3}{2}} d\sigma_{\mathbb{S}^{d-2}}(\eta) dt,$$

see [8, Eq. 1.16]. Furthermore, the uniform surface measure $\mathcal{U}_{\mathbb{S}^{d-1}}$ reads as

$$d\mathcal{U}_{\mathbb{S}^{d-1}}(\xi) = \frac{1}{s_{d-1}} (1 - t^2)^{\frac{d-3}{2}} d\sigma_{\mathbb{S}^{d-2}}(\eta) dt,$$

where s_{d-1} is the volume of \mathbb{S}^{d-1} . Hence

$$\begin{aligned} c_{d,r}^{-1} &= \int_{\mathbb{S}^{d-1}} |\xi_1|^r d\mathcal{U}_{\mathbb{S}^{d-1}}(\xi) = \frac{1}{s_{d-1}} \int_{\mathbb{S}^{d-2}} \int_{-1}^1 |t|^r (1 - t^2)^{\frac{d-3}{2}} dt d\sigma_{\mathbb{S}^{d-2}}(\eta) \\ &= \frac{s_{d-2}}{s_{d-1}} 2 \int_0^1 t^r (1 - t^2)^{\frac{d-3}{2}} dt = \frac{s_{d-2}}{s_{d-1}} B\left(\frac{r+1}{2}, \frac{d-1}{2}\right), \end{aligned} \quad (10)$$

where $B(z_1, z_2)$ is the beta function and we used the integral identity

$$B(z_1, z_2) = 2 \int_0^1 t^{2z_1-1} (1 - t^2)^{z_2-1} dt.$$

Finally, noting that $s_{d-1} = \frac{2\pi^{d/2}}{\Gamma(\frac{d}{2})}$ and $B(z_1, z_2) = \frac{\Gamma(z_1)\Gamma(z_2)}{\Gamma(z_1+z_2)}$, (10) can be computed as

$$c_{d,r}^{-1} = \frac{\Gamma(\frac{d}{2})}{\sqrt{\pi}\Gamma(\frac{d-1}{2})} \frac{\Gamma(\frac{r+1}{2})\Gamma(\frac{d-1}{2})}{\Gamma(\frac{r+d}{2})} = \frac{\Gamma(\frac{d}{2})\Gamma(\frac{r+1}{2})}{\sqrt{\pi}\Gamma(\frac{d+r}{2})}$$

Taking the inverse gives the claim. \square

B Proof of Theorem 2

In the first part of the proof, we will use properties of reproducing kernel Hilbert spaces (RKHS), see [70] for an overview on RKHS. For the second part, we will need two lemmata. The first one gives a definition of the MMD in terms of the Fourier transform (characteristic function) of the involved measures, where $\hat{\mu}(\xi) = \langle e^{-ix\xi}, \mu \rangle = \int_{\mathbb{R}^d} e^{-i\langle \xi, x \rangle} d\mu(x)$. Its proof can be found, e.g., in [72, Proposition 2]. Note that the constant on the right hand-side differs from [72, Proposition 2], since we use a different notion of the Fourier transform and the constant $\frac{1}{2}$ in the MMD.

Lemma 7. *Let $\mu \in \mathcal{P}_1(\mathbb{R})$ and $K(x, y) = -\|x - y\|$. Then it holds*

$$\mathcal{D}_K^2(\mu, \nu) = \frac{\Gamma(\frac{d+1}{2})}{2\pi^{\frac{d+1}{2}}} \int_{\mathbb{R}^d} \frac{|\hat{\mu}(\xi) - \hat{\nu}(\xi)|^2}{\|\xi\|^{1+d}} d\xi.$$

For the next lemma, recall that the cumulative density functions (cdf) of $\mu \in \mathcal{P}(\mathbb{R})$ is the function $F_\mu : \mathbb{R} \rightarrow [0, 1]$ defined by

$$F_\mu(x) := \mu((-\infty, x]) = \int_{\mathbb{R}} \chi_{(-\infty, x]}(y) d\mu(y), \quad \chi_A(x) = \begin{cases} 1, & \text{if } x \in A, \\ 0, & \text{otherwise.} \end{cases}$$

We will need that the *Cramer distance* between probability measures μ, ν with cdfs F_μ and F_ν defined by

$$\ell_p(\mu, \nu) := \left(\int_{\mathbb{R}} |F_\mu - F_\nu|^p dx \right)^{\frac{1}{p}},$$

if it exists. The Cramer distance does not exist for arbitrary probability measures. However, for $\mu, \nu \in \mathcal{P}_1(\mathbb{R})$ is well-known that

$$\ell_1(\mu, \nu) = \mathcal{W}_1(\mu, \nu) \quad (11)$$

and we have indeed $F_\mu - F_\nu \in L_2(\mathbb{R})$. The following relation can be found in the literature, see, e.g., [71]. However, we prefer to add a proof which clearly shows which assumptions are necessary.

Lemma 8. *Let $\mu, \nu \in \mathcal{P}_1(\mathbb{R})$ and $k(x, y) = -|x - y|$. Then it holds*

$$\ell_2(\mu, \nu) = \mathcal{D}_k(\mu, \nu).$$

Proof. By Lemma 7, we know that

$$\mathcal{D}_k^2(\mu, \nu) = -\frac{1}{2} \int_{\mathbb{R}} \int_{\mathbb{R}} |x - y| d(\mu - \nu)(x) d(\mu - \nu)(y) = \frac{1}{2\pi} \int_{\mathbb{R}} \frac{|\hat{\mu}(\xi) - \hat{\nu}(\xi)|^2}{\xi^2} d\xi. \quad (12)$$

For $\mu, \nu \in \mathcal{P}_1(\mathbb{R})$, we have $F_\mu - F_\nu \in L_2(\mathbb{R})$ and can apply Parseval's equality

$$\ell_2^2(\mu, \nu) = \int_{\mathbb{R}} |F_\mu(t) - F_\nu(t)|^2 dt = \frac{1}{2\pi} \int_{\mathbb{R}} |\hat{F}_\mu(\xi) - \hat{F}_\nu(\xi)|^2 d\xi. \quad (13)$$

Now we have for the distributional derivative of F_μ that $DF_\mu = \mu$, which can be seen as follows: using Fubini's theorem, we have for any Schwartz function $\phi \in \mathcal{S}(\mathbb{R})$ that

$$\begin{aligned} \langle DF_\mu, \phi \rangle &= -\langle F_\mu, \phi' \rangle = - \int_{\mathbb{R}} \int_{\mathbb{R}} \chi_{(-\infty, x]}(y) \phi'(x) d\mu(y) dx = - \int_{\mathbb{R}} \int_{\mathbb{R}} \chi_{(-\infty, x]}(y) \phi'(x) dx d\mu(y) \\ &= - \int_{\mathbb{R}} \int_y^\infty \phi'(x) dx d\mu(y) = \int_{\mathbb{R}} \phi(y) d\mu(y) = \langle \mu, \phi \rangle. \end{aligned}$$

Then we obtain by the differentiation property of the Fourier transform [59] that

$$\hat{\mu}(\xi) = \widehat{DF_\mu}(\xi) = -i\xi \hat{F}_\mu(\xi).$$

Finally, (13) becomes

$$\ell_2^2(\mu, \nu) = \frac{1}{2\pi} \int_{\mathbb{R}} \frac{|\hat{\mu}(\xi) - \hat{\nu}(\xi)|^2}{\xi^2} d\xi,$$

which yields the assertion by (12). \square

Now we can prove Theorem 2.

Proof. 1. To prove of the first inequality, we use the reproducing property

$$\langle f, \tilde{K}(x, \cdot) \rangle_{\mathcal{H}_{\tilde{K}}} = f(x)$$

of the kernel in the associated RKHS $\mathcal{H}_{\tilde{K}}$. For any $f \in \mathcal{H}_{\tilde{K}}$ with $\|f\|_{\mathcal{H}_{\tilde{K}}} \leq 1$ and any $\pi \in \Pi(\mu, \nu)$, we use the estimation

$$\begin{aligned} \left| \int_{\mathbb{R}^d} f(x) d(\mu - \nu)(x) \right| &= \left| \int_{\mathbb{R}^d} \int_{\mathbb{R}^d} f(x) - f(y) d\pi(x, y) \right| \leq \int_{\mathbb{R}^d} \int_{\mathbb{R}^d} |f(x) - f(y)| d\pi(x, y) \\ &= \int_{\mathbb{R}^d} \int_{\mathbb{R}^d} |\langle f, \tilde{K}(x, \cdot) - \tilde{K}(y, \cdot) \rangle_{\mathcal{H}_{\tilde{K}}}| d\pi(x, y) \\ &\leq \int_{\mathbb{R}^d} \int_{\mathbb{R}^d} \|\tilde{K}(x, \cdot) - \tilde{K}(y, \cdot)\|_{\mathcal{H}_{\tilde{K}}} d\pi(x, y), \end{aligned}$$

which is called “coupling bound” in [69, Prop. 20]. Then, since $\|\tilde{K}(x, \cdot) - \tilde{K}(y, \cdot)\|_{\mathcal{H}_{\tilde{K}}}^2 = \tilde{K}(x, x) + \tilde{K}(y, y) - 2\tilde{K}(x, y) = 2\|x - y\|$ and using Jensen’s inequality for the concave function $\sqrt{\cdot}$, we obtain

$$\left| \int_{\mathbb{R}^d} f(x) d(\mu - \nu)(x) \right| \leq \sqrt{2} \int_{\mathbb{R}^d} \int_{\mathbb{R}^d} \|x - y\|^{\frac{1}{2}} d\pi(x, y) \leq \left(2 \int_{\mathbb{R}^d} \int_{\mathbb{R}^d} \|x - y\| d\pi(x, y) \right)^{\frac{1}{2}}.$$

By the dual definition of the discrepancy $2\mathcal{D}_K(\mu, \nu) = \sup_{\|f\|_{\mathcal{H}_K} \leq 1} \int_{\mathbb{R}^d} f d(\mu - \nu)$, see [57], and taking the supremum over all such f and the infimum over all $\pi \in \Pi(\mu, \nu)$, we finally arrive at

$$2\mathcal{D}_K^2(\mu, \nu) \leq \mathcal{W}_1(\mu, \nu).$$

2. The second inequality can be seen as follows: by [14, Lemma 5.1.4], there exists a constant $c_d > 0$ such that

$$\mathcal{W}_1(\mu, \nu) \leq c_d R^{\frac{d}{d+1}} \mathcal{S}\mathcal{W}_1(\mu, \nu)^{\frac{1}{d+1}} = c_d R^{\frac{d}{d+1}} (\mathbb{E}_{\xi \sim \mathcal{U}_{\mathbb{S}^{d-1}}} [\mathcal{W}_1(P_{\xi\#}\mu, P_{\xi\#}\nu)])^{\frac{1}{d+1}}.$$

Further, we obtain by (11), the Cauchy-Schwarz inequality and Lemma 8 that

$$\begin{aligned} \mathbb{E}_{\xi \sim \mathcal{U}_{\mathbb{S}^{d-1}}} [\mathcal{W}_1(P_{\xi\#}\mu, P_{\xi\#}\nu)] &= \mathbb{E}_{\xi \sim \mathcal{U}_{\mathbb{S}^{d-1}}} [l_1(P_{\xi\#}\mu, P_{\xi\#}\nu)] \\ &\leq \mathbb{E}_{\xi \sim \mathcal{U}_{\mathbb{S}^{d-1}}} [(2R)^{\frac{1}{2}} l_2(P_{\xi\#}\mu, P_{\xi\#}\nu)] \\ &= (2R)^{\frac{1}{2}} \mathbb{E}_{\xi \sim \mathcal{U}_{\mathbb{S}^{d-1}}} [\mathcal{D}_k(P_{\xi\#}\mu, P_{\xi\#}\nu)] \\ &\leq (2R)^{\frac{1}{2}} (\mathbb{E}_{\xi \sim \mathcal{U}_{\mathbb{S}^{d-1}}} [\mathcal{D}_k^2(P_{\xi\#}\mu, P_{\xi\#}\nu)])^{\frac{1}{2}}, \end{aligned}$$

and finally by Theorem 1 that

$$\mathbb{E}_{\xi \sim \mathcal{U}_{\mathbb{S}^{d-1}}} [\mathcal{W}_1(P_{\xi\#}\mu, P_{\xi\#}\nu)] \leq (2R)^{\frac{1}{2}} \mathcal{D}_K(\mu, \nu) = (2R)^{\frac{1}{2}} \left(\frac{\Gamma(\frac{d}{2})}{\sqrt{\pi}\Gamma(\frac{d+1}{2})} \right)^{\frac{1}{2}} \mathcal{D}_K(\mu, \nu).$$

In summary, this results in

$$\mathcal{W}_1(\mu, \nu) \leq c_d \left(\frac{2\Gamma(\frac{d}{2})}{\sqrt{\pi}\Gamma(\frac{d+1}{2})} \right)^{\frac{1}{2(d+1)}} R^{\frac{2d+1}{2d+2}} \mathcal{D}_K(\mu, \nu)^{\frac{1}{d+1}}.$$

□

C Proof of Theorem 3

Interaction Energy: This part of the proof is similar to [73, Sec. 3]. Using that σ is a permutation and by reordering the terms in the double sum, we can rewrite the interaction energy by

$$\begin{aligned} E(\mathbf{x}) &= -\frac{1}{2N^2} \sum_{i=1}^N \sum_{j=1}^N |x_i - x_j| = -\frac{1}{2N^2} \sum_{i=1}^N \sum_{j=1}^N |x_{\sigma(i)} - x_{\sigma(j)}| \\ &= -\frac{1}{N^2} \sum_{i=1}^N \sum_{j=i+1}^N x_{\sigma(j)} - x_{\sigma(i)} = \sum_{i=1}^N \frac{N - (2\sigma(i) - 1)}{N^2} x_{\sigma(i)}. \end{aligned}$$

Since the x_i are pairwise disjoint, the sorting permutation σ is constant in a neighborhood of \mathbf{x} . Hence, E is differentiable with derivative

$$\nabla_{x_i} E(\mathbf{x}) = \frac{N + 1 - 2\sigma(i)}{N^2}.$$

Potential Energy: For any $x \neq y \in \mathbb{R}$ it holds

$$\nabla_x |x - y| = \chi(x, y), \quad \text{where} \quad \chi(x, y) = \begin{cases} 1, & \text{if } x > y, \\ -1, & \text{if } x < y. \end{cases}$$

Thus, we have that

$$\begin{aligned}\nabla_{x_i} V(\mathbf{x}|\mathbf{y}) &= \frac{1}{MN} \sum_{j=1}^M \chi(x_i, y_j) \\ &= \frac{1}{MN} (\#\{j \in \{1, \dots, M\} : y_j < x_i\} - \#\{j \in \{1, \dots, M\} : y_j > x_i\})\end{aligned}$$

Using that $\#\{j \in \{1, \dots, M\} : y_j > x_i\} = M - \#\{j \in \{1, \dots, M\} : y_j < x_i\}$ the above expression is equal to

$$\frac{1}{MN} (2 \#\{j \in \{1, \dots, M\} : y_j < x_i\} - M) = \frac{2 \#\{j \in \{1, \dots, M\} : y_j < x_i\} - M}{MN}.$$

□

D Proof of Theorem 4

In this section, we derive error bounds for the stochastic estimators for the gradient of MMD as defined in (6) for the Riesz kernel with $r = 1$. To this end, we employ concentration inequalities [74], which were generalized to vector-valued random variables in [41]. We will need the following Lemma which is the Bernstein inequality and is stated in [41, Lemma 18].

Lemma 9 (Bernstein Inequality). *Let X_1, \dots, X_P be independent random vectors with mean zero, $\|X_i\| \leq \mu$ and $\mathbb{E}[\|X_i\|_2^2] \leq \sigma^2$. Then it holds for $0 < t < \frac{\sigma^2}{\mu}$ that*

$$\mathbb{P}\left[\left\|\frac{1}{P} \sum_{i=1}^P X_i\right\|_2 > t\right] \leq \exp\left(-\frac{P t^2}{8\sigma^2} + \frac{1}{4}\right).$$

Now we can use Lemma 9 to show convergence of the finite sum approximation to the exact gradient.

Theorem 10 (Concentration Inequality). *Let $x_1, \dots, x_N, y_1, \dots, y_M \in \mathbb{R}^d$. Then, it holds*

$$\mathbb{P}\left[\|\tilde{\nabla}_P F_d(\mathbf{x}|\mathbf{y}) - \nabla F_d(\mathbf{x}|\mathbf{y})\| > t\right] \leq \exp\left(-\frac{P t^2}{32(c_d + 1)^2} + \frac{1}{4}\right).$$

Proof. Let $\xi_1, \dots, \xi_P \sim \mathcal{U}_{\mathbb{S}^{d-1}}$ be the independent random variables from the definition of $\tilde{\nabla}_P$ in (6). We set

$$X_{i,l} := c_d \nabla_l F_1(\langle \xi_i, x_1 \rangle, \dots, \langle \xi_i, x_N \rangle | \langle \xi_i, y_1 \rangle, \dots, \langle \xi_i, y_M \rangle) \xi_i$$

and define the dN -dimensional random vector $X_i = (X_{i,1}, \dots, X_{i,N})$. Then, we have by (4) that

$$\mathbb{E}[X_i] = \nabla F_d(\mathbf{x}|\mathbf{y}) = (\nabla_{x_1} F_d(\mathbf{x}|\mathbf{y}), \dots, \nabla_{x_N} F_d(\mathbf{x}|\mathbf{y})).$$

By Theorem 3, we know that $\|X_{i,l}\|_2 \leq \frac{2c_d}{N}$, and by (3) it holds

$$\|\mathbb{E}[X_{i,l}]\|_2 = \|\nabla_{x_l} F_d(\mathbf{x}|\mathbf{y})\|_2 \leq \frac{2}{N}.$$

Let $\tilde{X}_i = X_i - \mathbb{E}[X_i]$. Then it holds

$$\|\tilde{X}_i\|_2 \leq \sum_{l=1}^N \|\tilde{X}_{i,l}\|_2 \leq \sum_{l=1}^N \frac{2c_d + 2}{N} = 2c_d + 2$$

and thus $\mathbb{E}[\|\tilde{X}_i\|_2^2] \leq 4(c_d + 1)^2$. Since we have $\mathbb{E}[\tilde{X}_i] = 0$ for all $i = 1, \dots, P$, we can apply Lemma 9 and obtain

$$\mathbb{P}\left[\left\|\frac{1}{P} \sum_{i=1}^P X_i - \nabla F_d(\mathbf{x}|\mathbf{y})\right\| > t\right] = \mathbb{P}\left[\left\|\frac{1}{P} \sum_{i=1}^P \tilde{X}_i\right\| > t\right] \leq \exp\left(-\frac{P t^2}{32(c_d + 1)^2} + \frac{1}{4}\right).$$

Since we have by definition that

$$\frac{1}{P} \sum_{i=1}^P X_i = \tilde{\nabla}_P F_d(\mathbf{x}|\mathbf{y})$$

this yields the assertion. □

Finally we can draw a corollary which immediately shows Theorem 4.

Corollary 11 (Error Bound for Stochastic Gradients). *For $x_1, \dots, x_N, y_1, \dots, y_M \in \mathbb{R}^d$, it holds*

$$\mathbb{E}[\|\tilde{\nabla}_P F_d(\mathbf{x}|\mathbf{y}) - \nabla F_d(\mathbf{x}|\mathbf{y})\|] \leq \frac{\exp(1/4)\sqrt{32\pi}(\sqrt{d}+1)}{2\sqrt{2}P}.$$

Proof. Denote by X the random variable

$$X = \|\tilde{\nabla}_P F_d(\mathbf{x}|\mathbf{x}) - \nabla F_d(\mathbf{x}|\mathbf{y})\|.$$

Then, we have by Theorem 10 that

$$\mathbb{P}[X > t] \leq \exp\left(-\frac{P t^2}{32(c_d+1)^2} + \frac{1}{4}\right).$$

Thus, we obtain

$$\mathbb{E}[X] = \int_0^\infty \mathbb{P}[X > t] dt \leq \exp(1/4) \int_0^\infty \exp\left(-\frac{P t^2}{32(c_d+1)^2}\right) dt = \frac{\exp(1/4)\sqrt{32\pi}(c_d+1)}{2\sqrt{P}},$$

where the last step follows from the identity $\int_0^\infty \exp(-t^2) dt = \frac{\sqrt{\pi}}{2}$.

Now we proceed to bound the constant c_d in the dimensions. By Theorem 1 we have that $c_d = \frac{\sqrt{\pi}\Gamma(\frac{d+1}{2})}{\Gamma(\frac{d}{2})}$. Now the claim follows from the bound $\frac{\Gamma(\frac{d+1}{2})}{\Gamma(\frac{d}{2})} \leq \sqrt{\frac{d}{2}} + \sqrt{\frac{3}{4}} - 1$ proven in [37]. \square

E Comparison of Different Kernels in MMD

Next we compare the MMD flows of the Riesz kernels with those of the positive definite kernels

$$\begin{aligned} K_G(x, y) &:= \exp\left(-\frac{\|x-y\|^2}{2\sigma^2}\right) \quad (\text{Gaussian}), \\ K_{\text{IM}}(x, y) &:= \frac{1}{\sqrt{\|x-y\|^2 + c}} \quad (\text{Inverse Multiquadric}), \\ K_L(x, y) &:= \exp\left(-\frac{\|x-y\|}{\sigma}\right) \quad (\text{Laplacian}). \end{aligned}$$

The target distribution is defined as the uniform distribution on three non-overlapping circles and the initial particles are drawn from a Gaussian distribution with standard deviation 0.01, compare [24]. We recognize in Figures 5 and 6 that in contrast to the Riesz kernel, the other MMD flows

- heavily depend on the parameters σ and c (stability against parameter choice);
- cannot perfectly recover the uniform distribution; zoom into the middle right circles to see that small blue parts are not covered (approximation of target distribution).

Moreover, in contrast to the other kernels, the Riesz kernel with $r = 1$ is positively homogeneous such that the MMD flow is equivariant against scalings of initial and target measure.

Finally, it is interesting that the Riesz kernel is related to the Brownian motion by the following remark.

Remark 12. *In the one-dimensional case, the extended Riesz kernel with $r = 1$ reads as*

$$K(x, y) = -|x-y| + |x| + |y| = 2\min(x, y),$$

which is the twice the covariance kernel of the Brownian motion. More precisely, let $(W_t)_{t>0}$ be a Brownian motion and $s, t > 0$. Then, it holds

$$\text{Cov}(W_s, W_t) = \min(s, t) = \frac{1}{2}K(x, y).$$

F Ablation Study

We consider the FID for different number of networks and different number of projections. We run the same experiment as in Section 5 on MNIST. Here we choose a different number of projections P between 10 and 1000. In Figure 7 we illustrate the progress of the FID value for an increasing number of networks and a different number of projections. Obviously, the gradient of the MMD functional is not well-approximated by just using $P = 10$ or $P = 100$ projections and thus the MMD flow does not converge. Once the gradient of the functional is well-approximated, a higher number of projections leads only to a small improvement, see the difference between $P = 500$ and $P = 1000$.

G Implementation Details

We use UNets $(\Phi)_{l=1}^L$ with 3409633 trainable parameters for MNIST and FashionMNIST and 2064035 trainable parameters for CIFAR10. The networks are trained using Adam [38] with a learning rate of 0.001. All flows are simulated with a step size $\tau = 1$. We stop the training of our generative sliced MMD flow when the FID between the generated samples and some validation samples does not decrease twice. The validation samples are the last 10000 training samples from the corresponding

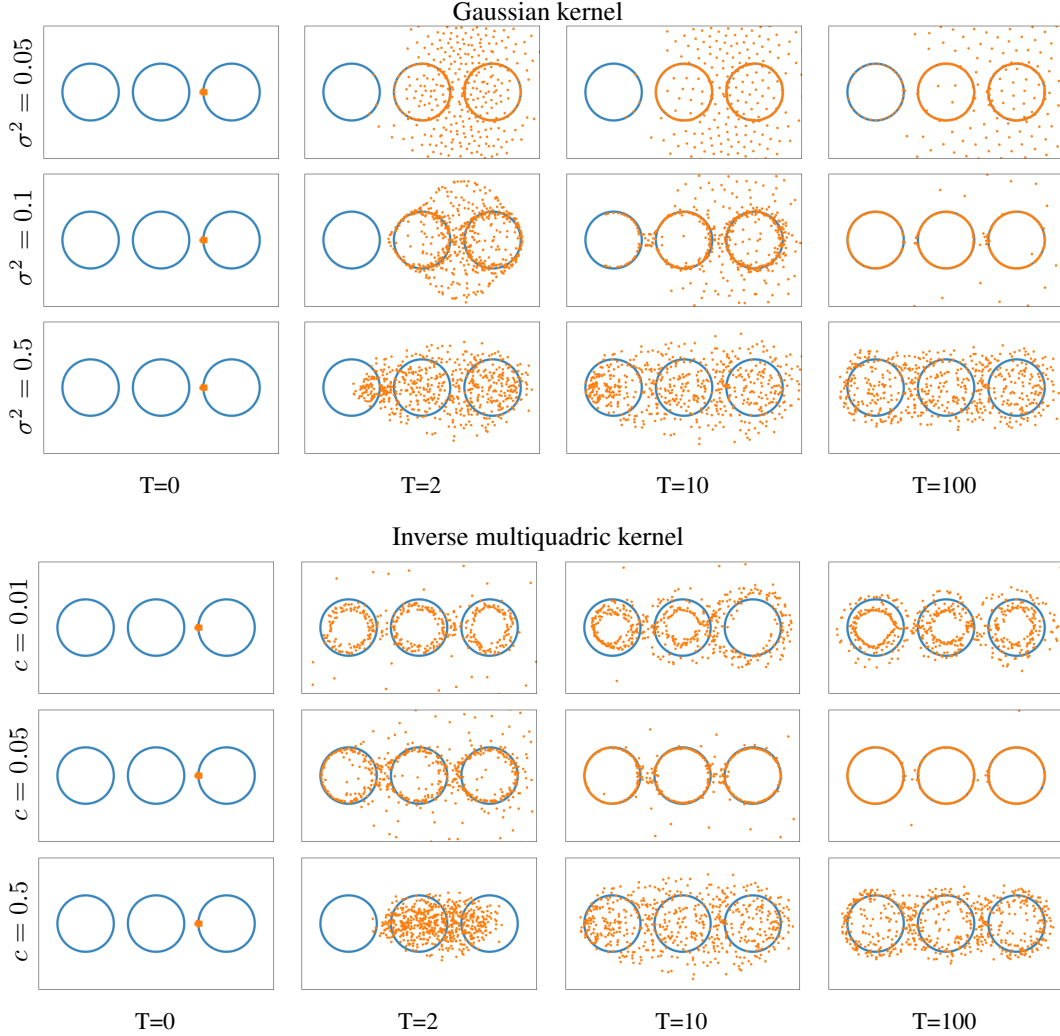


Figure 5: Comparison of the MMD flow with Gaussian kernel (top) and inverse multiquadric kernel (bottom) for different hyperparameters.

dataset which were not used for training the generative sliced MMD flow. The training of the generative MMD flow takes between 1.5 and 3 days on a NVIDIA GeForce RTX 2060 Super GPU, depending on the current GPU load by other processes.

MNIST We draw the first $M = 20000$ target samples from the MNIST training set and $N = 20000$ initial samples uniformly from $[0, 1]^d$. Then we simulate the momentum MMD flow using $P = 1200$ projections for 500 steps and train the network for 3000 optimizer steps with a batch size of 100. After each training of the network, we increase the number of flow steps by 1000 up to a maximal number of 30000 steps and we choose the momentum parameter $m = 0.85$. We stop the whole training after $L = 36$ networks.

FashionMNIST Here we draw the first $M = 20000$ target samples from the FashionMNIST training set and $N = 20000$ initial samples uniformly from $[0, 1]^d$. Then we simulate the momentum MMD flow using $P = 1000$ projections for 100 steps and train the network for 2000 optimizer steps with a batch size of 100. After each training of the network, we increase the number of flow steps by 200 and 1000, if the current step of the flow is smaller than 2000 and 20000, respectively, and by 2000 else. The maximal number of flow steps is set to 15000. The momentum parameter m is again increased after each network training by 0.05 up to 0.8, beginning with $m = 0$ in the first flow step. We stop the whole training after $L = 90$ networks.

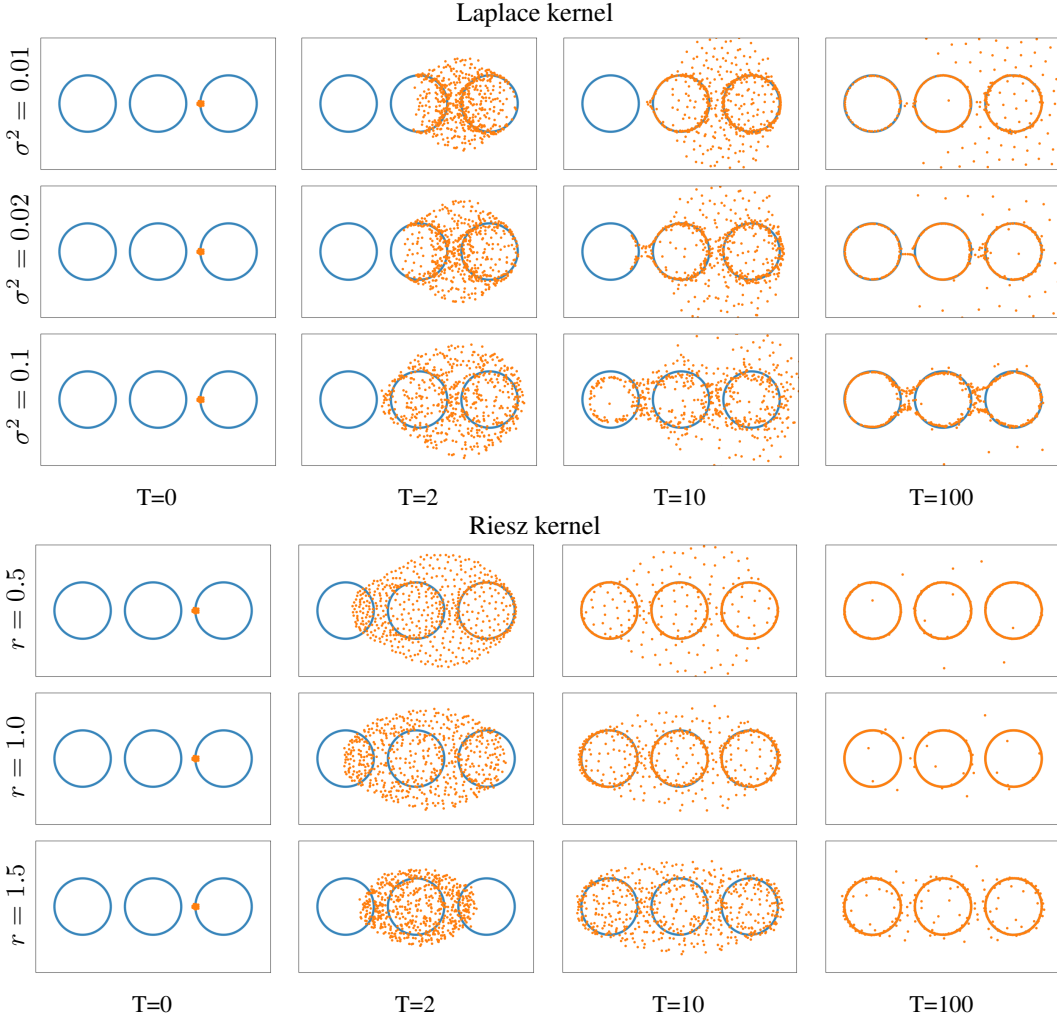


Figure 6: Comparison of the MMD flow with Laplacian kernel (top) and Riesz kernel (bottom) for different hyperparameters.

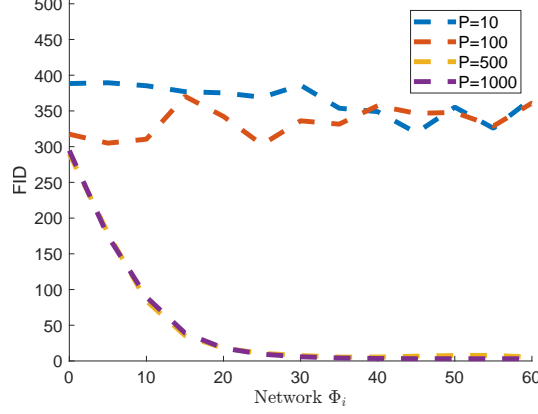


Figure 7: Illustration of the FID value of the Sliced MMD Flow on MNIST for different number of projections.

CIFAR We draw the first $M = 10000$ target samples from the CIFAR10 training set and $N = 10000$ initial samples uniformly from $[0, 1]^d$. Then we simulate the momentum MMD flow using $P = 4000$ projections for 200 steps and train the network for 2000 optimizer steps with a batch size of 100. After each training of the network, we increase the number of flow steps by 200 and 1000, if the current step of the flow is smaller than 1000, 10000, and by 2000 else. The maximal number of flow steps is set to 50000. The momentum parameter m is again increased after each network training by 0.05 up to 0.9, beginning with $m = 0$ in the first flow step. We stop the whole training after $L = 47$ networks.